

Screened hybrid and self-consistent GW calculations of cadmium/magnesium indium sulfide materials

Melissa J. Lucero,¹ Irene Aguilera,² Cristian V. Diaconu,¹ Pablo Palacios,^{2,3} Perla Wahnón,² and Gustavo E. Scuseria^{1,4}

¹*Department of Chemistry, Rice University, Houston, Texas 77005-1892, USA*

²*Instituto de Energía Solar and Departamento Tecnologías Especiales, ETSI Telecomunicación, UPM, Ciudad Universitaria, Madrid E-28040, Spain*

³*Física y Química Aplicadas a la Técnica Aeronáutica, E. de Ingeniería Aeronáutica y del Espacio, UPM, Ciudad Universitaria, Madrid E-28040, Spain*

⁴*Department of Physics and Astronomy, Rice University, Houston, Texas 77005-1827, USA*

(Received 14 February 2011; revised manuscript received 4 April 2011; published 25 May 2011)

The cadmium and magnesium indium sulfides are medium-gap semiconductors demonstrating a propensity to form intermediate band materials when doped with transition metals. The inherent structural diversity exhibited by $M^{+2}\text{In}_2\text{S}_4$ thiospinels and related AB_2X_4 compounds often precludes definitive experimental determination of the band-gap width and type of transition. Employing a series of traditional semilocal functionals (e.g., the local spin density approximation; the Perdew, Burke, and Enzerhof functional; and the Tao, Perdew, Staroverov, and Scuseria functional) the screened hybrid of Heyd, Scuseria, and Ernzerhof (HSE), band gaps, projected densities of states, and band structures are calculated for the normal, full inverse, and intermediate configurations of $[\text{Cd/Mg}]_8\text{In}_{16}\text{S}_{32}$. Band structures and band gaps are also obtained via self-consistent many-body methods, using the static Coulomb-hole and screened exchange approximation to GW as a starting point for perturbative G_0W_0 calculations. Comparison to experiment indicates that HSE provides an accurate, computationally efficient, and relatively rapid means for predicting band-gap properties in spinel-type photovoltaic materials.

DOI: [10.1103/PhysRevB.83.205128](https://doi.org/10.1103/PhysRevB.83.205128)

PACS number(s): 71.15.Mb, 71.20.Nr, 78.20.Bh

I. INTRODUCTION

Photovoltaic cells containing intermediate band (IB) materials are capable of efficiently absorbing photons over a broad range of the solar spectrum. An IB optimally situated between the valence and conduction bands can result in electron promotion using two photons with a combined energy expenditure *smaller* than the typical one-photon electronic excitation across the analogous semiconductor gap, boosting ideal efficiencies from 40.7%¹ to 63.1%.² Rapid prescreening of semiconductors with ~ 2 –3 eV band gaps will facilitate selection, suggest modification, and expedite fabrication of IB-forming, doped semiconductors.

To date, the majority of solid-state computational studies employ semilocal³ exchange correlation functionals [e.g., local spin density approximation (LSDA), generalized-gradient approximation (GGA), or meta-GGA variants] that consistently fail to reproduce experimental band gaps despite the development of more sophisticated approximations.⁴ Intermediate band photovoltaics are formally metallic, yet still closely resemble the undoped parent semiconductors that tend to have underestimated band gaps on the order of 1 eV.^{5–9}

Fortunately, more accurate results, comparable to those of full, self-consistent (sc) GW calculations,¹⁰ are accessible, at reduced computational cost, by employing the Coulomb-hole and screened exchange (COHSEX)^{11,12} approximation. The COHSEX approximation accounts for statically screened exchange and correlation in the form of the classical interaction between and additional point charge in the system and the surrounding polarization cloud that this additional charge induces. The static COHSEX result is then augmented with dynamic effects through a perturbative G_0W_0 calculation. The main effects neglected by this scheme are the excitonic and polaronic effects.

The scCOHSEX+ G_0W_0 (sc GW) scheme has been successfully applied to a wide range of materials,^{11,13–16} yielding *fundamental* band gaps (as opposed to the smaller *optical* gaps) and band structures, often in good agreement with experiment. Nevertheless, when applied to IB materials doped with high concentrations of transition metals, even these many-body corrections become prohibitively expensive for all but the smallest systems.¹⁷

Other well-established, less CPU-intensive corrections are also unsuitable for modeling transition-metal-doped IB materials: perturbative G_0W_0 after LSDA cannot accurately address the influence of populated d orbitals on band gaps,^{11,18} while density functional theory plus Hubbard U (DFT+ U) methods require system-dependent parameters that are unknown for novel materials. It is worth noting that the screened short-range Hartree-Fock exchange interactions in the hybrid functional of Heyd, Scuseria, and Ernzerhof^{19–21} (HSE) are reminiscent of the role that the Hubbard on-site repulsion U plays in DFT+ U . However, unlike + U methods, HSE can allocate a unique effective “ U ” to different orbital interactions. In fact, a recent paper²² advocates the use of HSE to determine U when experimental information is lacking and the need to reduce computational effort surmounts the desire for increased prediction quality. Significantly, HSE *alone* produces semiconductor band gaps and lattice parameters in excellent agreement with experiment,^{19,23} without requiring multiple calculations, perturbative adjustments or material-dependent parameters—and at significantly reduced cost relative to many-body corrections.^{13,14,24–26}

Recently, the $M^{+2}\text{In}_2\text{S}_4$ semiconductors containing Mg and Cd, garnered considerable attention due to their potential application in high-efficiency solar cells.^{6,27} Spinel-type chalcogenides are capable of adopting a variety of related crystalline forms,²⁸ a consequence of the AB_2X_4 lattice affording the

anions freedom to expand or contract around their fractional coordinates, thus allowing facile accommodation of a wide range of cation sizes, while maintaining overall symmetry. The literally hundreds of known spinels are classified according to the 24 occupied interstices of the fcc lattice (defined by X). By convention, the eight smaller, usually divalent cations occupying T_d holes are designated A , while the remaining 16, typically higher-valent B cations reside in O_h holes²⁹ yielding crystallographic unit cells of composition $A_8B_{16}X_{32}$, where $X = \text{O, S, Se, or Te}$.

The limiting designations³⁰ for cation occupancy in spinel structures are (a) *normal*, with all A cations filling T_d sites and all B cations in O_h holes, or (b) *full inverse*, in which $A = B$ for occupied O_h sites, forcing half of the B cations into T_d holes. The term *partial inverse* describes the spectrum of intermediate spinel structures, $x = A_{1-x}B_x[A_xB_{2-x}]X_4$, where brackets denote O_h sites. Thus defined, the degree of inversion, x , ranges from 0 (normal) to 1 (full inverse), with $x = \frac{2}{3}$ representing a fully stochastic system.

II. COMPUTATIONAL METHODS

A. Density functional calculations

Electronic-structure calculations were performed using the periodic boundary-condition code^{31–33} within the GAUSSIAN suite of programs.³⁴ Data analysis and visualization were performed using GaussView³⁵ and VMD.³⁶

Gaussian basis sets modified for solids are provided in the supplementary material³⁷ and are of the following quality: Mg: 8-511G (all-electron); S: 6-311G*(all-electron); Cd: 6-311G (all-electron); In: 4s4p2d (ECP, modified). Unless otherwise noted, initial geometries are the conventional, crystallographic unit cells ($Fd\bar{3}m$, 227), downloaded as CIF files from the ICSD,³⁸ The 56-atom crystallographic unit cells are optimized in redundant internal coordinates³⁹ with 36 \mathbf{k} points on a $4 \times 4 \times 4$ mesh for the reciprocal space integration. The 14-atom primitive cells are optimized similarly, but employ 112 \mathbf{k} points on a $6 \times 6 \times 6$ mesh.

Reported band gaps and related properties for fully relaxed (lattice parameters and geometries) periodic systems were obtained using three semilocal and one screened hybrid functional to create a series of increasingly sophisticated exchange-correlation approximations. Specifically, we compare the local spin density approximation (LSDA)⁴⁰ (with SVWN5⁴¹), the GGA corrected functional of Perdew, Burke, and Enzerhof^{42,43} (PBE), the meta-GGA functional of Tao, Perdew, Staroverov, and Scuseria⁴⁴ (TPSS), and the nonlocal Heyd-Scuseria-Enzerhof⁴⁵ screened hybrid functional (HSE).

B. Many-body calculations

All many-body calculations were performed on 14-atom cells using the plane-wave based code ABINIT.⁴⁶ For the COHSEX and G_0W_0 calculations,⁴⁷ a basis set of ~ 25000 plane waves was required for convergence. A Monkhorst-Pack \mathbf{k} -point mesh of $3 \times 3 \times 3$ was used to sample the Brillouin zone. Norm-conserving pseudopotentials⁴⁸ were generated with the *fhi98PP* code,⁴⁹ accounting for *semicore states* (e.g., the 4s4p4d of In) explicitly in the valence, following Hybertsen.⁵⁰ Details of the pseudopotential generation

procedure can be found in the supplementary material.³⁷ The plasmon-pole model⁵¹ is used for G_0W_0 calculations and COHSEX wave functions are represented on a restricted LSDA basis set as proposed by Bruneval.¹¹ All *scGW* calculations start from relaxed LSDA-optimized structures: normal $\text{Cd}_2\text{In}_4\text{S}_8$, $a_o = 10.775 \text{ \AA}$; normal $\text{Mg}_2\text{In}_4\text{S}_8$, $a_o = 10.682 \text{ \AA}$; full inverse $\text{Mg}_2\text{In}_4\text{S}_8$, $a_o = 10.634 \text{ \AA}$.

III. CADMIUM INDIUM SULFIDE

Numerous applications, particularly in photovoltaics and light-emitting diodes (LED's),^{52–54} render cadmium indium sulfide an extremely well-studied thiospinel, generally accepted to crystallize in a *normal* structure, with $x \approx 1$, although studies involving partial inverse structures and mixed crystals have been reported.^{55,56} DFT calculations of normal CdIn_2S_4 were performed on the conventional 56-atom crystallographic unit cells ($Fd\bar{3}m$, 227), as well as the 14-atom primitives. The inverse ordering is modeled using only the primitive cells.

A. Cd normal spinel structure

Measured band gaps are on the order of 2.1–2.7 eV.^{52,57–66} A rather broad range of band gaps is also observed for the related spinel-type transparent conducting oxides (TCO's) CdIn_2O_4 , $E_g = 2.67\text{--}3.24$,⁶⁷ and Cd_2SnO_4 , $E_g = 2.06\text{--}3.00$.^{67,68} Comparison of bulk and thin-film specimens of the $\text{Cd}_{1+x}\text{In}_{2-2x}\text{Sn}_x\text{O}_4$ solid solution demonstrates that the optical gaps for thin films are significantly larger than for bulk samples,⁶⁹ this difference most likely arising from a Burstein-Moss shift.⁷⁰ Furthermore, the gap narrows as the cation ordering becomes more inverted,⁷¹ a consequence of the order-disorder phenomena discussed in Sec. IV. Note that there are many documented *larger* lattice constants than the commonly cited $a_o = 10.797$. Lee *et al.*⁶⁰ report that the CdIn_2S_4 a_o varies according to the method of crystal growth, ranging from 10.838 to 10.860 \AA , rather larger than the 10.797 \AA reported by Hahn.⁷² Thus, the band-gap widths for these systems are affected by dimensionality and degree of inversion, which is dependent upon method of synthesis: films have larger gaps, and any reaction condition that facilitates inversion results in lower gaps.

As indicated in Table I, the three semilocal functionals underestimate the gap for the normal spinel by at least 1 eV, as expected, while the screened hybrid HSE provides band gaps close to that of experiment at 2.33 eV, tending toward the bottom of the reported experimental band gaps. There is also an experimental lack of consensus (see Ref. 73 and references therein) regarding the *nature* of the transition. However, all four functionals predict an *indirect* transition that is ~ 10 meV lower in energy than that for the direct path, perhaps indicating that this minor energy difference is somehow related to the general disagreement regarding the type of band gap. (The common practice of reporting only one decimal place induces a coalescence of theoretical gaps, thus forcing inference of a *direct* gap.) This vanishingly small ΔE is not unique: $\beta\text{-In}_2\text{S}_3$ also has experimental band gaps ranging from 2 to 3 eV in magnitude with disputed indirect-direct transitions typically varying by ~ 10 meV.⁷⁴ Note that the $\beta\text{-In}_2\text{S}_3$ structure can

TABLE I. Normal and full inverse CdIn₂S₄: Functional dependence of band gap (eV) and lattice parameters (Å).

Functional	LSDA		PBE		TPSS		HSE	
	E_i	E_d	E_i	E_d	E_i	E_d	E_i	E_d
Nature of gap								
Normal	Cd ₈ In ₁₆ S ₃₂				56-atom cell			
Experiment	2.2–2.7 ^a		$a_o = 10.797^b$					
a_o	10.840		11.106		11.073		11.000	
Band gap ^c	1.34	1.44	1.21	1.28	1.52	1.60	2.33	2.41
Rlx→HSE _{sp} ^d	2.14	2.25	2.13	2.21	2.19	2.28		
Full inverse	Cd ₂ In ₄ S ₈				14-atom cell			
a	7.671		7.861		7.835		7.776	
b	7.722		7.909		7.883		7.841	
c	7.656		7.842		7.813		7.763	
Band gap ^c	0.21	0.22	0.13	0.14	0.37	0.40	1.19	1.23
Rlx→HSE _{sp} ^d	1.39	1.42	1.02	1.06	1.08	1.11		

^aReferences 52,57–66.

^bICSD ID 300725.⁷²

^cFully relaxed geometry and forces.

^dRelaxed using LSDA/PBE/TPSS and then HSE energy calculation.

be considered a parent of the many indium thiospinels, and it is often described as a quaternary defect spinel with cationic vacancies in the T_d sites ordered along the c axis.⁷⁵

The 0 K lattice parameters predicted by LSDA most closely resemble measured values, yet the HSE-relaxed geometry, with a slightly larger volume, has a band gap in much better agreement with experiment. In fact, while LSDA geometries are generally considered to be better for semiconductors, the UV photoemission spectra of CdIn₂S₄ and related spinels exhibit little sensitivity to small crystallographic deviations.⁷⁶ Full relaxation using each of the semilocal functionals, followed by HSE single point energy calculations, is summarized in the “Rlx→HSE_{sp}” row of Table I. All relaxed lattices, with a_o varying from experiment by 4–30 pm, result in gaps close to—or within—the experimental range, clearly illustrating the profound effect that the introduction of nonlocal Hartree-Fock-type exchange has on bandwidth.

Moreover, the HSE single point energy of the LSDA-relaxed structure, with a gap of 2.14 eV, and the HSE-relaxed gap of 2.33 eV are at the bottom of the experimental range, which correctly corresponds to bulk^{58,59} rather than thin-film^{52,53} band gaps. Indeed, a recent study of hierarchical nanostructured CdIn₂S₄ produced at low temperatures using different methods resulted in multiple morphologies, yet the band gaps were constrained to a narrow range of 2.23–2.27 eV.⁷⁷

Admittedly, evaluation of Hartree-Fock exchange is computationally expensive for *any* hybrid functional. This potential bottleneck may be surmounted by first performing a full relaxation with a less expensive functional, followed by a single point energy calculation using HSE. This simple shortcut yields more accurate band gaps and would work equally well for *any* functional considered to produce superior lattice parameters, whether traditionally semilocal or next-generation, designed specifically for solids, e.g., HSEsol.⁷⁸ This procedure should prove quite useful, particularly for studies of formation energies of interstitial defects,⁷⁹ defect transition levels⁸⁰ (HSE performs particularly well for both),

or any investigation requiring large supercells. Moreover, this shortcut is possible in any software package with an implementation of HSE.

B. Cd full inverse spinel structure

The experimentally unobserved full inverse structure (bottom section, Table I), like the normal spinel, also has a marginally indirect band gap, predicted to have a width of 0.1–0.4 eV by all functionals except HSE, which produces a somewhat larger, 1.2 eV gap. The HSE single point energies of structures relaxed using semilocal functionals also show an increased in gap, with the indirect transition favored, again, by only a milli-electron volt. Notably, the analogous spinel oxide, CdIn₂O₄, was also calculated to have a smaller band gap in the inverse spinel structure.⁸¹ HSE thus provides an interesting prediction of a 1.2–1.4 eV band gap should such a structure be isolated.

C. Densities of states

The Cd₈In₁₆S₃₂ normal spinel projected density of states (PDOS) is plotted for each functional in Fig. 1. The In 5s (blue) and S 3p orbitals (yellow) dominate the conduction band, while the primary contribution to the valence band is almost exclusively S 3p orbital. This pattern is strikingly similar to that observed for β -In₂S₃, which has a gap of around 2.1 eV.^{82,83} The Cd 5s contribution is minimal in both the top of the valence and bottom of the conduction bands, demonstrating that metal insertion into the β -In₂S₃ manifold produces more significant structural consequences (ordered defect spinel → normal spinel) than for electronic properties relevant to the band gap. As the exchange correlation approximations improve, LSDA → TPSS, a clear blueshift is observed for the conduction band, which dramatically increases upon introduction of nonlocal Hartree-Fock exchange (HSE). In contrast, very little of interest transpires in the valence band, which is somewhat wider for HSE than the semilocal functionals. The HSE band resembles that for LSDA, but has more structure and a slightly extended (~0.2–0.3 eV) low-energy tail.

The transition from normal to full inverse spinel structures results in a marked decrease in the predicted band gaps—from 2.3 to 1.2 eV—and both the valence and conduction bands broaden and change morphology, as is illustrated in Fig. 2. Further, a small band on the edge of the low-energy tail of the conduction band appears in both spinels, which is discernible in the bottom of Fig. 2, between 1 and 2 eV (2 and 3 eV in the normal spinel). Enlargements of these regions are depicted in Fig. 3 to facilitate comparison of the HSE PDOS. While the In 5s orbitals predominate in both cases, the enlargements indicate that this small, almost isolated, feature closely resembles the larger section of the conduction band, yet the relative contributions of the sulfur and cadmium orbitals change. In the normal spinel, Figs. 3(a) and 3(c), the sulfur 3s, 3p, and Cd 5s orbital contributions are nearly identical, while in the full inverse structure, Figs. 3(b) and 3(d), the sulfur 3s contribution increases as does that of the In 4d orbitals, which were not present in the tail of the normal spinel (c) at all.

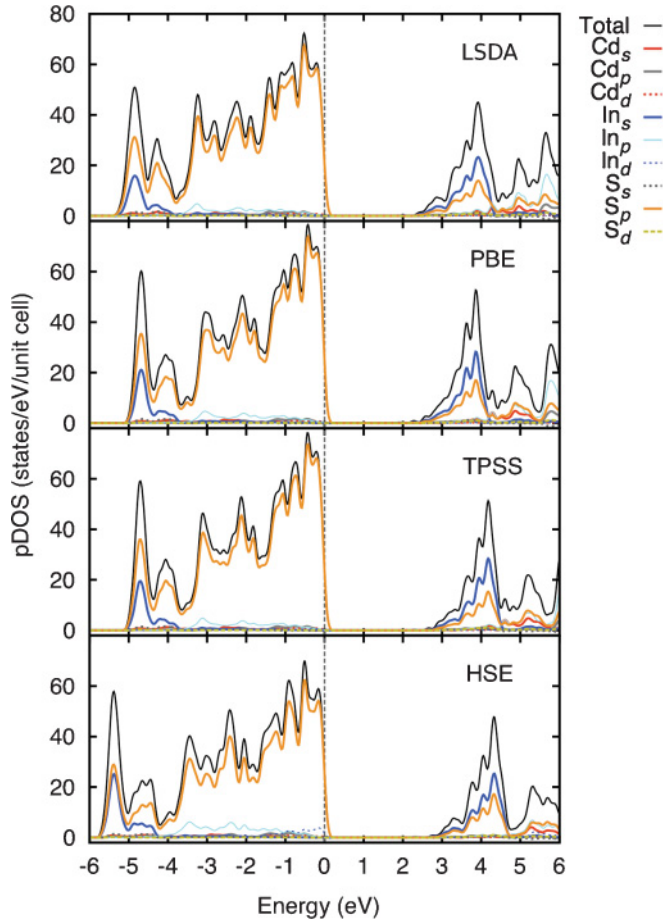


FIG. 1. (Color online) Projected density of states for $\text{Cd}_8\text{In}_{16}\text{S}_{32}$ as a normal spinel structure, calculated with LSDA, PBE, TPSS, and HSE. The Fermi level is indicated by the dashed black line at $E = 0$. The top of the valence band does not terminate exactly at zero due to a 10 meV Gaussian line broadening.

IV. MAGNESIUM INDIUM THIOSPINELS

While observed in a natural spinel, MgAl_2O_4 , the normal structure is not adopted by many synthetic Mg-containing spinel oxides.^{84,85} As already discussed, this dependence of configuration upon the method of formation and synthesis is also observed for many thiospinels, including those with $A = \text{Mg}$,⁸⁶ and is consequence of the oxygen or chalcogenide anions forming a highly adaptable fcc structure, allowing a wide range of cations to not only occupy, but move in between the T_d and O_h holes. This structural mobility is influenced by the chemical composition, but is more sensitive to the ordering of occupied holes, which, in turn, varies according to cation size, electrostatic interactions, structure defects, and temperature.^{87,88} Experimental determination of the *ground-state* cation distributions is thus nontrivial, particularly since the high temperatures requisite for most older spinel syntheses mimic the formation conditions of the natural minerals known to form metastable crystalline states,⁸⁹ and consequent adherence to Ostwald's rule.⁹⁰ At lower temperatures, thermal equilibrium is also difficult to obtain due to very low diffusion rates.⁹¹

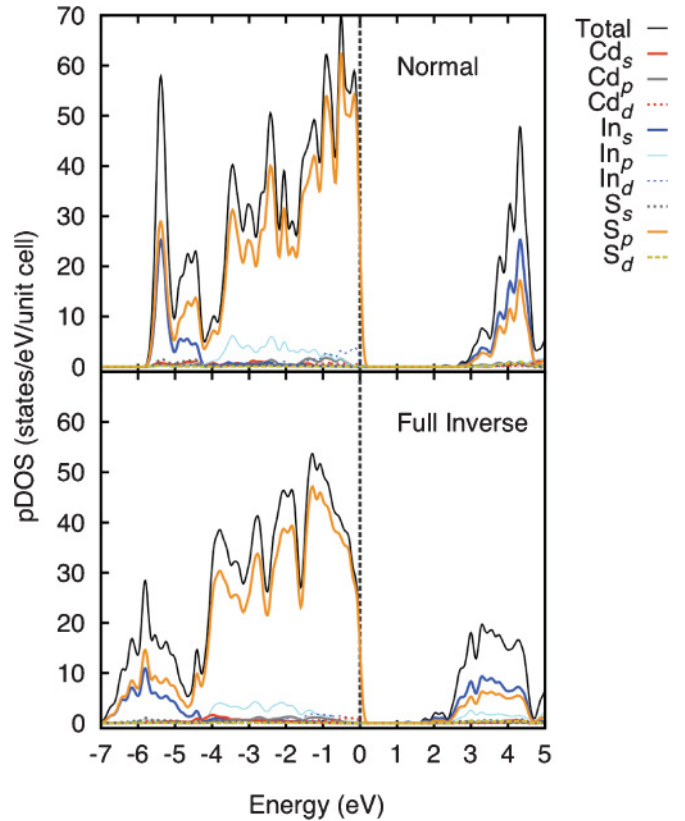


FIG. 2. (Color online) The HSE projected density of states for $\text{Cd}_8\text{In}_{16}\text{S}_{32}$ in normal (top) and full inverse (bottom) spinel structures. The Fermi level is indicated by the dashed black line at $E = 0$. The top of the valence band does not terminate exactly at zero due to a 10 meV Gaussian line broadening.

Not surprisingly, several *order-disorder* phenomena⁹² have been recognized in spinels. The normal spinels generally exhibit long-range, nonconvergent order-disorder behavior, in which the extent of inversion changes continuously without a phase transition, while inverse spinels exhibit two types of order-disorder behavior: (1) an ordered inverse \rightarrow disordered inverse first-order transition stabilized by configurational entropy-associated cation exchange in O_h sites, or (2) a nonconvergent disordered inverse to another disordered state stabilized entropically by cation exchange in both T_d and O_h sites.⁹³

The stability of the normal versus inverse structures, for Cd/Mg In_2S_4 , assuming low-temperature thermal equilibrium is presented in Table II. From a 0 K perspective, the Cd system makes sense thermodynamically, implying that a normal structure should predominate, assuming thermal equilibrium is achieved. Recall from Sec. III that experimentally, normal (or close to normal) structures are observed and a full inverse analog has not been isolated.

For the Mg thiospinels, the energy preference between either inverse ordering and the normal structure is significantly reduced. This is not surprising, as both MgIn_2S_4 and its oxide equivalent, MgIn_2O_4 , are observed to adopt some form of inverse structure.⁸⁶ The partial inverse configuration is calculated to be *less* stable than the full inverse, yet experimentally, a fully inverse structure has not been isolated.

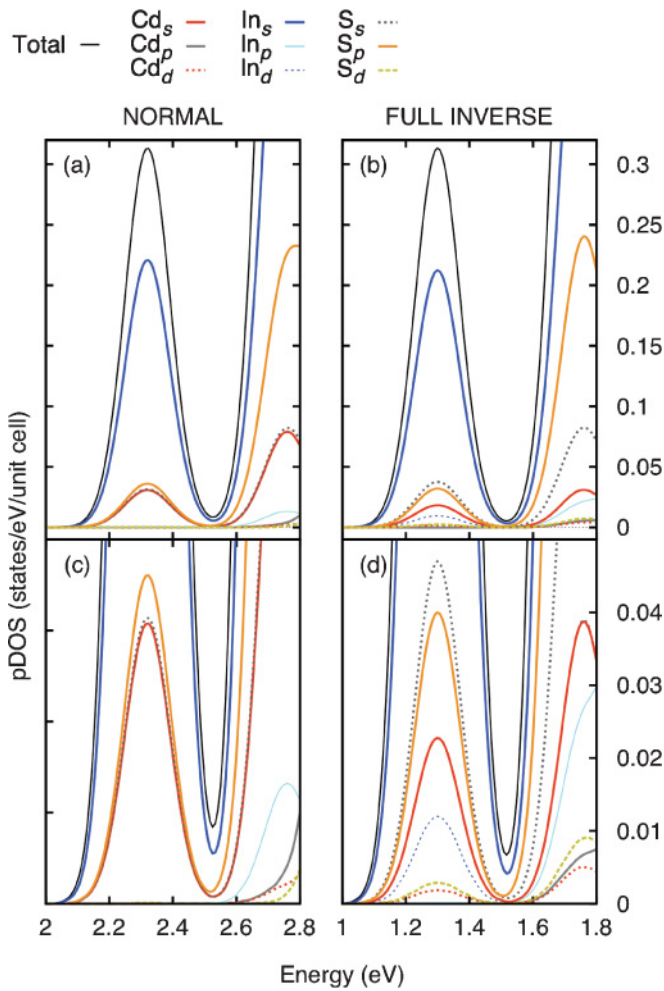


FIG. 3. (Color online) Enlargement of the low-energy region in the conduction bands of the HSE projected density of states for $\text{Cd}_8\text{In}_{16}\text{S}_{32}$ adopting normal (left) and full inverse (right) spinel structures. The top figures (a) and (b) highlight the similar band shapes, but somewhat different population densities, while the increased zoom in the bottom plots (c) and (d) further illustrate the disparate contributions from the relevant S, Cd, and In orbitals as the spinel structure is inverted.

Nevertheless, MgGa_2O_4 , a spinel with an experimental degree of inversion similar to our partial inverse structure (~ 0.84),⁹⁴ was shown via finite-temperature MC calculations,⁹¹ to prefer an inverse-type structure at RT , strongly implying that synthetic MgIn_2S_4 is subject to some form of order-disorder

TABLE II. $M^{2+}\text{In}_2\text{S}_4$ relative energies by type (kcal/mol).

Functional Spinel type	Functional			
	LSDA	PBE	TPSS	HSE
MgIn_2S_4				
Normal	0.00	0.00	0.00	0.00
Partial inverse	4.60	3.27	3.02	3.37
Full inverse	4.13	2.67	2.42	2.15
CdIn_2S_4				
Normal	0.00	0.00	0.00	0.00
Full inverse	17.01	17.00	17.49	16.57

behavior. Recent specialized models⁹⁵ and finite-temperature simulations⁹⁶ demonstrate that predicting whether a normal or inverse-type ordering scheme will predominate in the 0–278 K range and identifying the relative stability of the three disordered states possible for inverse structures is complex and labor-intensive.⁹⁷

Fortunately, there is abundant experimental data for $\text{Mg}_8\text{In}_{16}\text{S}_{32}$, so we simulate cation distributions by using the 56-atom crystallographic unit cell as a template to construct the normal, partial, and full inverse orderings, shown as (a), (b), and (c), respectively, in Fig. 4. All structures started with an approximate $Fd\bar{3}m$ symmetry prior to full relaxation.

A. Mg normal spinel structure

The heretofore unobserved *normal*-type $\text{Mg}_8\text{In}_{16}\text{S}_{32}$ is the structure available from crystallographic databases and it is also the easiest to benchmark computationally. The results of several theoretical studies^{61,73,98,99} also provide an alternate means for comparison in the absence of experimental data. The DFT predictions are summarized in Table III.

Paralleling the Cd system, all functionals produce fully relaxed $\text{Mg}_8\text{In}_{16}\text{S}_{32}$ cells with *expanded* lattice parameters, LSDA deviating the least. The band gap is observed to increase as the cation ordering approaches the normal extreme for the analogous oxide,^{81,100} and the Cd thiospinel also followed this pattern, so it is reasonable to expect the Mg *normal* spinel will also have a larger gap. The experimentally observed band gaps for the Mg system correspond to what is known to be a partial inverse configuration (see Table V), implying that the normal band gap should be *larger* than 2.1–2.3 eV. In fact, HSE predicts a band gap of 2.83 eV—similar in magnitude to the high end 2.7 eV of reported Cd thiospinel gaps. The three semilocal functionals all produce smaller gaps, thus $\text{HSE} > \text{TPSS} > \text{LSDA} > \text{PBE}$. Whether one references the smaller partial inverse measured gaps or trusts the larger HSE prediction paralleling the Cd system (Table I), errors are on the order of 20%–30%.

These data indicate again that the presence of nonlocal Hartree-Fock exchange in the calculation far outweighs any lattice differences: indeed, LSDA predicts the smallest relaxed volume as well as the narrowest gap, whereas TPSS has a much larger a_o , yet still fails to produce a band gap of the magnitude predicted by HSE, and PBE has the largest cell but the smallest

TABLE III. Normal $\text{Mg}_8\text{In}_{16}\text{S}_{32}$: Functional dependence of band gap (eV) and lattice parameters (Å).

Functional	LSDA		PBE		TPSS		HSE	
	E_i	E_d	E_i	E_d	E_i	E_d	E_i	E_d
$\text{Mg}_8\text{In}_{16}\text{S}_{32}$								
Experiment	$a_o = 10.687^a$							
a_o	10.715		10.935		10.898		10.840	
Band gap ^b	1.73		1.69		2.01		2.83	
$\text{Rlx} \rightarrow \text{HSE}_{\text{sp}}^c$	2.88		2.63		2.71			

^aICSD ID 59551.⁷²

^bFully relaxed geometry and forces.

^cHSE energy calculation of fully-relaxed structure.

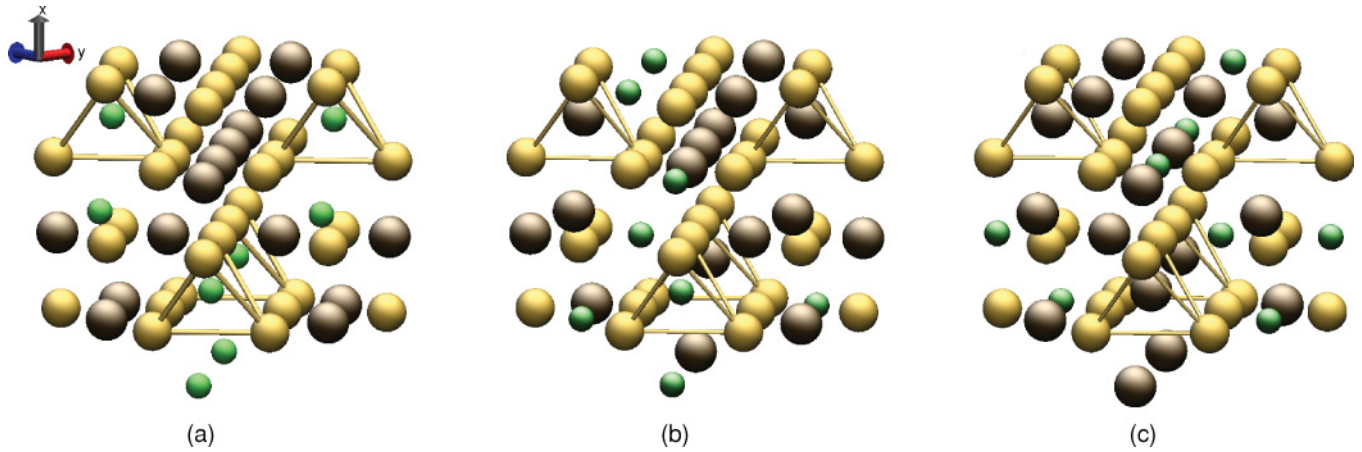


FIG. 4. (Color online) The three 56-atom conventional, crystallographic unit cells addressing cation ordering for $Mg_8In_{16}S_{32}$ in this study: the (a) normal, (b) partial inverse, and (c) full inverse spinel structures. The Mg^{+2} cation is green, In^{+3} is brown, and the S^{-2} anion is yellow. Cations in T_d holes are surrounded by yellow tetrahedra.

band gap. The HSE single point calculations on the structures relaxed using semilocal functionals provide larger gaps, all within ~ 0.2 eV of the HSE prediction.

Comparison of the normal spinel PDOS for the four functionals is presented in the column to the far left of Fig. 5. Again paralleling the Cd thiospinel, the valence band is dominated by the sulfur $3p$ orbitals, with minor contributions from the indium $5p$ and $4d$ orbitals. The conduction band

is also dominated by indium $5s$ and sulfur $3p$ orbitals in nearly equal amounts. The population patterns remain more or less the same, and a blueshift is again evident. *Unlike* the Cd system, there is no extra structure observed at the edge of the low-energy tail of the conduction band, and all four functionals predict that the band gap is *direct*. Nevertheless, a normal spinel structure for $Mg_8In_{16}S_{32}$ has yet to be isolated, so the HSE band gap of 2.83 is purely predictive.

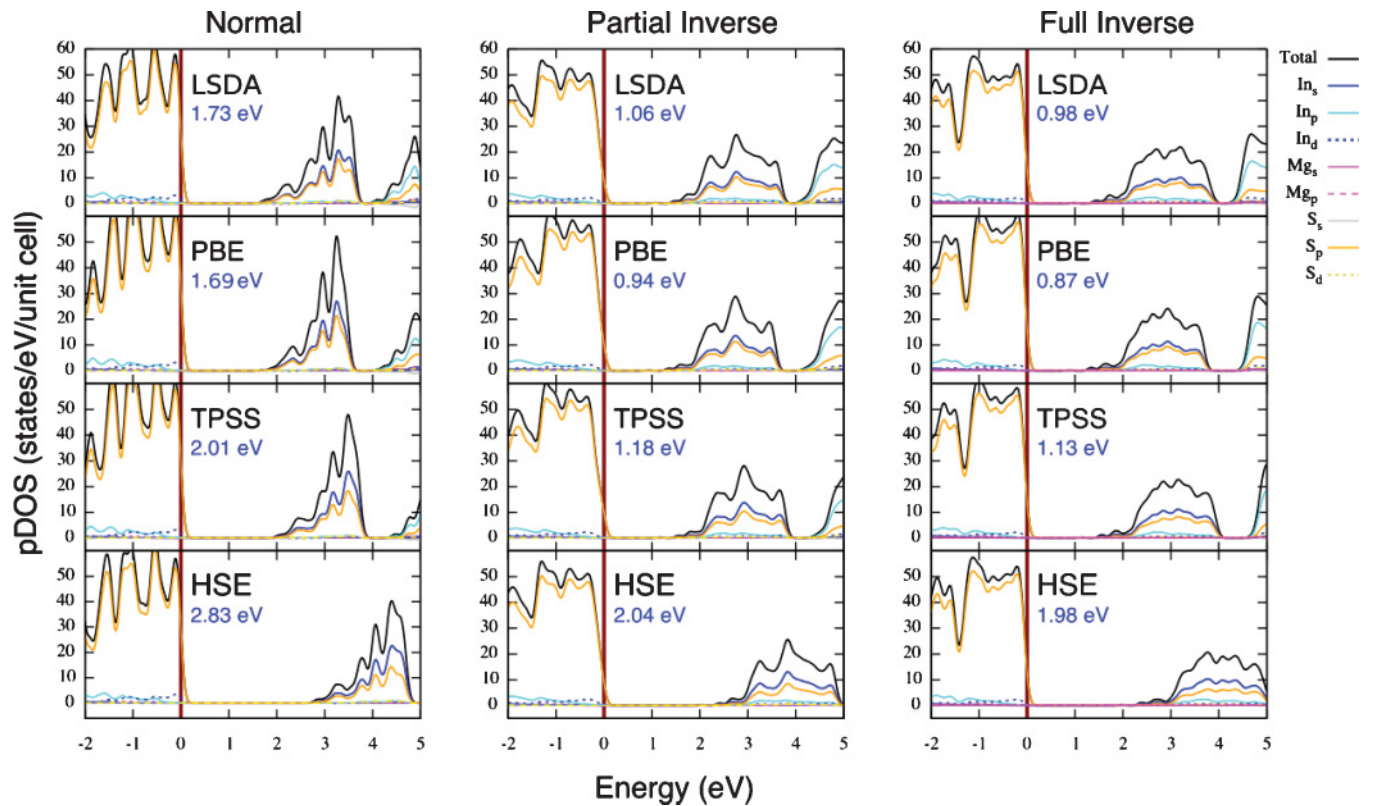


FIG. 5. (Color online) Projected density of states for $Mg_8In_{16}S_{32}$ for the normal, partial inverse, and full inverse spinel structures as calculated using LSDA, PBE, TPSS, and HSE. The Fermi level is indicated by the dark red line at $E = 0$. The top of the valence band does not terminate exactly at zero due to a 10 meV Gaussian line broadening.

TABLE IV. Full inverse $\text{Mg}_8\text{In}_{16}\text{S}_{32}$: Functional dependence of band gap (eV) and lattice parameters (\AA).

Functional	LSDA		PBE		TPSS		HSE	
	E_i	E_d	E_i	E_d	E_i	E_d	E_i	E_d
Nature of gap								
$\text{Mg}_8\text{In}_{16}\text{S}_{32}$								
Experiment	2.1–2.3 ^a				$a_0 = 10.687^a$			
a	10.674		10.904		10.867		10.802	
b	10.680		10.910		10.873		10.809	
c	10.677		10.906		10.869		10.804	
Band gap ^b	0.98	1.04	0.87	0.91	1.13	1.18	1.98	2.04

^aICSD ID 59551,⁷² with 8 Mg and 8 In exchanged.

^bFully relaxed (geometry and forces) 56-atom cells.

B. Mg full inverse spinel structure

A fully inverse structure is also unobserved in nature or synthetically, but serves as a close approximation to experiment ($x = 1$ versus $x = 0.84$) facilitating direct comparison. As is evident from Table IV, all functionals predict an *indirect* band gap; the semilocal functions severely underestimate the gap, while HSE yields 1.98 eV, slightly below the experimental range of 2.1–2.3 eV, which is reasonable given that the partial inverse gap should be larger. LSDA predicts a slightly contracted lattice, analogous to what is observed for the Cd analog, while all other functionals predict an expansion. The HSE lattice parameters again show the smallest increase in volume.

Cursory visual inspection reveals several striking contrasts in both the shape and populations of the calculated PDOS in Fig. 5 for the normal (far left) and full inverse (far right) thiospinels. In the normal configuration, the valence band has considerable structure, which is drastically attenuated in the full inverse motif. As with the Cd compounds, the normal spinel conduction band has a slowly diminishing tail and a maximum near the high-energy edge of the conduction band, whereas the full inverse conduction band has a more symmetrical population density and an overall smoother “band shape.” In general, both structure types exhibit similar contributions from the sulfur 3*p* (yellow) and indium 4*d* orbitals (blue). However, the indium 5*p* orbitals (cyan), observed primarily in the valence band of the normal spinel, also show a non-negligible presence in the *conduction* band of the full inverse spinel. This increased In 5*p* contribution can be considered a migration from the high-energy band beginning at ~ 4 eV (LSDA) in the normal structure, into the lower-energy conduction band of the full inverse structure. Finally, the magnesium 3*s* orbitals (magenta) are seen to contribute—albeit marginally—to both the valence and conduction bands for full-inverse ordering, while not at all, at least in the bands of relevance to the gap, for normal ordering. These dramatic changes in population densities are evident for HSE as well as the semilocal functionals—the main distinction being the increasingly wider band gaps.

C. Partial inverse spinel structure

Most characterizations of synthetic $\text{Mg}_8\text{In}_{16}\text{S}_{32}$ report a *partial inverse* structure.^{58,60,101–105} An intermediate degree of inversion for the 56-atom, full fcc conventional unit cell

TABLE V. Partial inverse Mg In thiospinels: Functional dependence of band gap (eV) and lattice parameters (\AA).

Functional	LSDA		PBE		TPSS		HSE	
	E_i	E_d	E_i	E_d	E_i	E_d	E_i	E_d
Nature of gap								
$\text{Mg}_8\text{In}_{16}\text{S}_{32}^a$								
Experiment	2.1–2.3 ^b				$a_0 = 10.687^c$			
a	10.698		10.927		10.889		10.827	
b	10.689		10.919		10.888		10.817	
c	10.694		10.922		10.878		10.822	
Band gap	1.06	1.08	0.94	0.95	1.18	2.04	2.06	
Full inverse ^c	0.98	1.04	0.87	0.91	1.13	1.18	1.98	2.04

^aStarted with Ref. 72, see text for ordering description, $x \approx$ ICSD ID 59551.

^bReferences 58,61,102,103,105 and 106.

^c $\text{Mg}_8\text{In}_{16}\text{S}_{32}$ from Table IV.

$\text{Mg}_8\text{In}_{16}\text{S}_{32}$ was obtained by taking the structure of Hahn⁷² and swapping six cations. Specifically, two In^{3+} are moved from O_h to T_d holes, with four O_h holes swapped with Mg^{2+} “randomly” according to their order in the input file to produced a normality of $x = 0.84$.^{102,106} Table V summarizes relevant data for the partial inverse MgIn_2S_4 structure. Predictions for the full inverse structure are also included for ease of reference.

As expected, the gaps for full and partial inverse structures are of similar magnitude and the gap is indirect. The semilocal results underestimate the gap by at least 1 eV, whereas the HSE prediction is within 6 meV of the lower bound for the *RT* experimental values of 2.14 eV.¹⁰³ Interestingly, low-temperature (4 K) experiments indicate an indirect transition across a gap of 2.26 eV, which is 14 meV lower than the direct transition.^{104,107} A gap of ~ 2.1 eV suggests that a *partial inverse* structure should be a dark red color, which is, in fact, what is observed.^{58,106} This vanishingly small energy difference is also observed in the cubic tin indium thio spinel,¹⁰⁸ several zinc spinels [e.g., ZnRh_2O_4 (Ref. 109) or ZnGa_2O_4 (Ref. 110)], and the parent β -indium sulfide structure:⁷⁴ in all cases, the band gaps are ~ 2 –3 eV with a disputed band-gap type.

Comparison of both inverse structure PDOS’s in Fig. 5 (center and right columns) demonstrates the degree of similarity between the partial and full inverse Mg thiospinels. The population densities are similar for both inverse structures, and HSE exhibits patterns resembling those produced by the semilocal functionals. Alas, the systems are not identical. Closer examination of the conduction band (HSE) reveals that Mg *s* orbitals contribute slightly more in the peak of the tail for the partial inverse structure, Fig. 6 (top), which is also slightly blueshifted with respect to the full inverse structure, Fig. 6 (bottom), where Mg *p* orbitals begin to contribute. This enlargement demonstrates that there is also generally more Mg *s*- and *p*-orbital contribution in the conduction band for the full inverse structure. At higher energies, the partial inverse structure shows redshifted indium *p*, *d*, and sulfur *s* orbitals, and noticeable orbital-ordering-by-contribution differences occur at 2.5, 2.9, and 3.0 eV in the conduction band. Note that there is no such contribution in the normal spinel configuration as there is no additional structure at the bottom of the

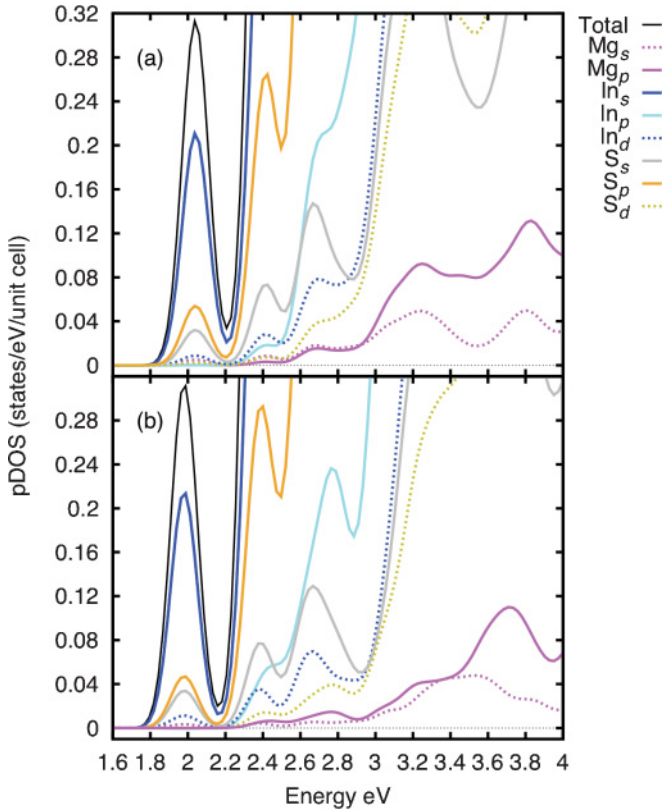


FIG. 6. (Color online) HSE projected density of states for $\text{Mg}_8\text{In}_{16}\text{S}_{32}$ for the (a) partial inverse and (b) full inverse spinel structures. The bottom of the conduction band is enlarged to illustrate dissimilar population patterns. Each plot uses 10 meV Gaussian line broadening.

conduction band, and the Mg contribution (left column, Fig. 5) is primarily at the higher end of the conduction band, not near the band gap.

The spinel systems are clearly disordered systems.^{29,93} When the shape of the optical absorption edge is exponential, producing “Urbach tails,”¹¹¹ information about the degree of disorder can be inferred. In recent investigations of the disorder in α -silicon,¹¹² the calculated DOS and fitting for tails bear a striking resemblance to what is observed in spinels.⁵⁸ While the valence band in all Cd/Mg thiospinels is sharply terminated, the conduction band has exponential tails. The inverse structures are necessarily more disordered while the normal Cd thiospinel would be more disordered than the unknown Mg analog (which shows no extra band) because of the larger cation.

V. MANY-BODY CALCULATIONS OF THIOSPINELS

The 14-atom $M^{+2}\text{In}_2\text{S}_4$ primitives for Cd and Mg were relaxed using LSDA. Corrected band gaps for the normal Cd, normal Mg, and full inverse spinel structures were obtained using a $\text{scCOHSEX}+G_0W_0$ many-body treatment (see Sec. II). Symmetry considerations require a 56-atom unit cell for the partial inverse structure, which is not computationally feasible for scGW , but as was shown previously, properties of the intermediate structure can be inferred from the behavior of the limiting structures, particularly that of the full inverse

structure. The Fermi level is taken to be zero in all plots. For comparison, the same primitives were optimized using HSE.

The resulting band structures are presented in Fig. 7, with the scGW and HSE bands on top and bottom, respectively. It is immediately evident that the scGW and HSE band structures are very similar. Further, all calculated band structures, regardless of ordering, exhibit a flat, nondisperse character in the valence band and exhibit a high degree of structure in the conduction band—a pattern typically observed for spinel oxides.^{113–115}

In the conduction band, the Cd and Mg cations adopting the normal configuration (left and right columns of Fig. 7) display slightly different structure than those of the Mg full inverse ordering (center column), particularly along the $\mathbf{W} \rightarrow \mathbf{K}$ path, where the bands show less curvature, notably around \mathbf{L} . It is interesting that the *experimentally observed* Cd normal (right) and Mg inverse (center) structures manifest similar curvature at the bottom of the conduction band, with a clear separation of the In 5s and slightly higher in energy S 3s orbitals. In contrast, the same bands of the unobserved Mg normal compound [Figs. 7(c) and 7(e)] overlap.

In terms of band gaps, both scGW and HSE predict an *indirect* transition for the normal Cd compound [Figs. 7(a) and 7(d), respectively]. The scGW correction locates the valence-band maximum along the $\mathbf{K} \rightarrow \mathbf{\Gamma}$ path yielding an indirect gap of 2.98 eV, while HSE predicts a gap of 2.33 eV along the same path.

For the full inverse Mg compound, scGW predicts an *indirect* transition, spanning a 3.04 eV gap that originates from the valence-band maximum in the $\mathbf{K} \rightarrow \mathbf{\Gamma}$ direction. The scGW gap is overestimated by ~ 1 eV relative to experiment (Table VI) and the flat top of the valence band conceals the fact that the indirect gap is only 10 meV lower than the direct transition. On the other hand, the smaller HSE band gap underestimates experiment by only ~ 0.3 eV. While the HSE prediction is somewhat lower than the experimental range for a *known* partial inverse structure, this is to be expected—the

TABLE VI. Normal and full inverse $\text{Mg}_2\text{In}_4\text{S}_8$: scGW band gaps (eV) compared to four functionals.

Functional	LSDA		PBE		TPSS		HSE	
	E_i	E_d	E_i	E_d	E_i	E_d	E_i	E_d
Nature of gap								
Cd normal								
Expt.	2.2–2.7 ^a							
Band gap ^b	1.34	1.43	1.21	1.30	1.52	1.59	2.33	2.41
scGW^c	2.98	3.10						
Mg normal								
Band gap ^d	1.75		1.69		2.01		2.84	
scGW^c	3.85							
Mg full inverse								
Expt.	2.1–2.2 ^e							
Band gap ^d	0.96		0.85		1.12		1.93	
scGW^c	3.04	3.05						

^aFully relaxed 14-atom cells. ICSD ID 300725.⁷²

^bReferences 52,57–66.

^c14-atom *normal* spinel cell, initially relaxed using LSDA.

^dICSD ID 59551.⁷²

^eUsing partial inverse structure data: Refs. 58,61,102,103,105,106.

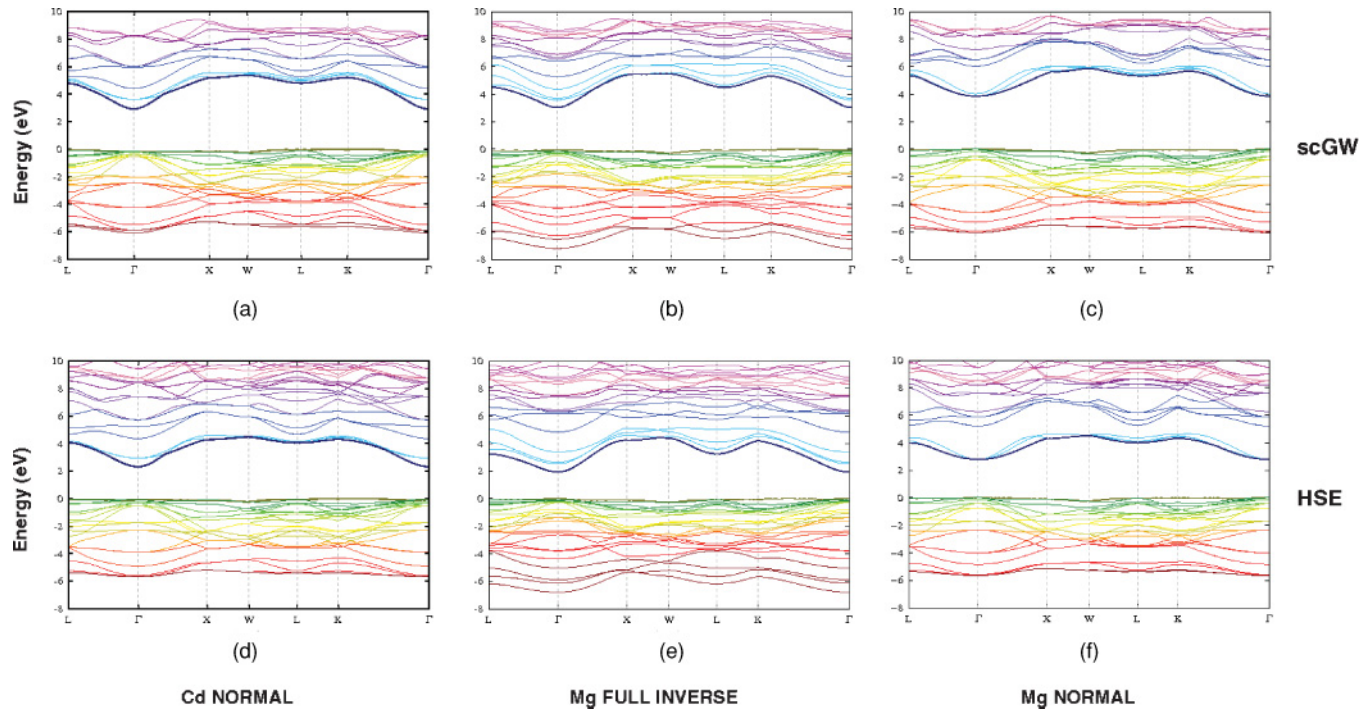


FIG. 7. (Color online) Comparison of *scGW* (top) and HSE (bottom) band structures for the Cd/Mg indium thiospinels along the $\mathbf{L}\Gamma\mathbf{X}\mathbf{W}\mathbf{L}\mathbf{X}\mathbf{\Gamma}$ path. Normal $\text{Cd}_2\text{In}_4\text{S}_8$ spinel (a) and (d); full inverse $\text{Mg}_2\text{In}_4\text{S}_8$ spinel (b) and (e), and the *predicted* normal spinel ordering for $\text{Mg}_2\text{In}_4\text{S}_8$ (c) and (f).

scGW error would also be expected to decrease slightly if a true partial inverse, not a full inverse structure, was examined. The small energetic distinction between indirect and direct gaps does not exist for HSE, nor any of the DFT calculations, when using the smaller, 14-atom primitives, as it did for the 56-atom conventional cells (Tables III and IV), which is not surprising considering the magnitude of $\Delta E_{\text{dir}} - E_{\text{ind}}$ and the reduction of information inherent to using a smaller system with fewer electrons.

In the last case, the purely theoretical Mg normal structure, *scGW* predicts a direct band gap with a magnitude of 3.85 eV. HSE also predicts a direct transition, but the band gap is narrower at 2.84 eV. Nevertheless, the *scGW* and HSE bands strongly resemble each other (right column of Fig. 7). As there are no experimental data for comparison, these gaps remain exclusively predictive, but the HSE band gap is, as was pointed out earlier (see Sec. IV A), very reasonable.

A. Discussion

For the known Cd and Mg compounds, the difference between experiment and *scGW* is opposite in sign, but nearly equal in magnitude to the error that LSDA and GGA typically show for these systems.^{73,99} While the *scGW* scheme used in this work is known to overestimate indirect semiconductor band gaps,¹¹⁶ the ~ 1 eV disparity is somewhat larger than the expected 0.1–0.3 eV.¹¹ There are, however, numerous factors (beyond the precision of the method itself) with the potential to create this large disparity between *scGW* predictions and experimental measurements.

The most likely issue is probably the neglect of excitonic effects: in medium-gap materials, screening is lower and the

electron-hole interaction becomes stronger.¹¹⁷ Although there is no clear experimental evidence supporting the presence of an excitonic effect, the absorption spectra of Ruiz-Fuertes *et al.*⁵⁸ might support this hypothesis. Polaronic effects, which are also absent in *scGW*¹⁴ methods and also show some dependence on the system,¹¹⁸ may also be relevant. While again unverified experimentally, significant polaronic effects are expected from the large $\epsilon_0 - \epsilon_\infty$ that these spinels present [$\epsilon_0 = 18.8\text{--}20.74$, $\epsilon_\infty = 5.5\text{--}5.8$ for MgIn_2S_4 (Refs. 103, 119) and $\epsilon_0 = 18.71$, $\epsilon_\infty = 6.49$ for CdIn_2S_4 (Ref. 120)]. Recently, Vidal¹²¹ showed that neglecting polaronic effects in many-body approaches can lead to band-gap overestimations of up to 1 eV. To a lesser extent, the differences between the LSDA and the experimental structural parameters (not only the lattice parameter a but also the ratio c/a and the internal anion distortion u), the finite temperature of the experiments, and the presence of other types of defects in the experimental samples (such as silica¹⁰³ or Mg vacancies¹¹⁹) may also contribute. The combined contributions of these otherwise small effects may explain why *scGW* consistently overestimates Cd/Mg indium thiospinels by ~ 1 eV. Nevertheless, recent reports of the successful application of HSE + G_0W_0 for band structures^{122,123} suggest an interesting alternative for future exploration.

VI. CONCLUSION

The indium thiospinels of Mg and Cd were examined by a theoretical treatment consisting of DFT and *scGW* many-body corrections to LSDA. Investigation into the relative performance of LSDA, PBE, TPSS, and HSE reaffirms earlier observations that semilocal functionals underestimate the band

gaps of these semiconductors, regardless of cation ordering, while demonstrating that the screened hybrid HSE provides band gaps and lattice parameters consistently in excellent agreement with experiment. It is also evident that the predictive power of HSE extends beyond the idealized extrema of normal and full inverse spinel occupancies through successful predictions for an experimentally observed partial inverse spinel structure.

The DFT calculations also indicate that while LSDA geometries are generally considered to be better, spinel-type band gaps are far more sensitive overall to the amount of nonlocal Hartree-Fock exchange than they are to pm scale deviations in the lattice parameters. The projected DOS illustrates that the presence of Hartree-Fock exchange induces a significant blueshift in the location of the bottom conduction band—regardless of the M^{+2} metal present. For all functionals, the conduction band also exhibits distinctive morphological changes as the degree of inversion increases from normal to full inverse, indicating population redistribution to lower states. In the valence band, the sulfur $3p$ orbitals provide the dominant contribution, while the conduction band consists primarily of the In $5s$ orbitals, followed closely by the sulfur $3p$ orbitals—a pattern strikingly similar to that of β - In_2S_4 .

The *scGW* analysis of band structures reveals that the method overestimates thiospinel band gaps, relative to both experiment and HSE, yet the structure and dispersion patterns of the *scGW* bands resemble those for other experimentally characterized spinel systems, as well as paralleling the predictions from the more expedient and accurate HSE

calculations. Both *scGW* and HSE predict a minute, meV-scale energetic distinction between indirect and direct transitions that is observed for isolable spinel compounds, regardless of configuration type and irrespective of the identity of the M^{+2} cation. Additionally, the strong agreement between the many-body and screened hybrid band structures implies that the details of reliable spinel band structure might serve as a useful adjunct to experimental determination of cation ordering because the normal and inverse spinels manifest dissimilar band patterns.

Thus, this combined DFT/*scGW* study confirms that the screened hybrid HSE provides an accurate, computationally efficient means for predicting band gaps for the structurally complex Cd/Mg indium sulfide semiconductors.

ACKNOWLEDGMENTS

The work at Rice was funded by the Department of Energy (Grant No. DE-FG02-09ER16053) and The Welch Foundation (C-0036). The Spanish effort was supported by the Ministerio de Ciencia y Innovación: Consolider Ingenio 2010 GENESIS-FV (Grant No. CSD2006-04), FOTOMAT (Grant No. MAT2009-14625-C03-01), and the Comunidad de Madrid NUMACIA 2 project (Grant No. S-2009ENE-1477). The authors thankfully acknowledge the computer resources and technical expertise provided by the Centro de Supercomputación y Visualización de Madrid (CeSViMa) and the Spanish Supercomputing Network.

-
- ¹W. Shockley and H. J. Queisser, *J. Appl. Phys.* **32**, 510 (1961).
- ²A. Luque and A. Martí, *Phys. Rev. Lett.* **78**, 5014 (1997).
- ³J. P. Perdew and K. Schmidt, *Jacob's Ladder of Density Functional Approximations for the Exchange-Correlation Energy*, in *Density Functional Theory and Its Applications to Materials*, edited by V. E. Van Doren, K. Van Alsenoy, and P. Geerlings (AIP, Melville, NY, 2001), pp. 1–20.
- ⁴G. E. Scuseria and V. N. Staroverov, *Theory and Applications of Computational Chemistry: The First 40 Years* (Elsevier, Amsterdam, 2005).
- ⁵I. Aguilera, P. Palacios, and P. Wahnón, *Thin Solid Films* **516**, 7055 (2008).
- ⁶R. Lucena, I. Aguilera, P. Palacios, P. Wahnón, and J. C. Conesa, *Chem. Mater.* **20**, 5125 (2008).
- ⁷P. Palacios, K. Sánchez, J. C. Conesa, J. J. Fernández, and P. Wahnón, *Thin Solid Films* **515**, 6280 (2007) see also U.S. Patent 6444897.
- ⁸P. Palacios, P. Wahnón, S. Pizzinato, and J. C. Conesa, *J. Chem. Phys.* **124**, 014711 (2006).
- ⁹P. Wahnón and C. Tablero, *Phys. Rev. B* **65**, 165115 (2002).
- ¹⁰S. V. Faleev, M. van Schilfhaarde, and T. Kotani, *Phys. Rev. Lett.* **93**, 126406 (2004).
- ¹¹F. Bruneval, N. Vast, and L. Reining, *Phys. Rev. B* **74**, 045102 (2006).
- ¹²L. Hedin, *Phys. Rev.* **139**, A796 (1965).
- ¹³J. Vidal, S. Botti, P. Olsson, J.-F. Guillemoles, and L. Reining, *Phys. Rev. Lett.* **104**, 056401 (2010).
- ¹⁴J. Vidal, F. Trani, F. Bruneval, M. A. L. Marques, and S. Botti, *Phys. Rev. Lett.* **104**, 136401 (2010).
- ¹⁵M. Gatti, F. Bruneval, V. Olevano, and L. Reining, *Phys. Rev. Lett.* **99**, 266402 (2007).
- ¹⁶F. Bruneval, N. Vast, L. Reining, M. Izquierdo, F. Sirotti, and N. Barrett, *Phys. Rev. Lett.* **97**, 267601 (2006).
- ¹⁷I. Aguilera, Ph.D. thesis, Universidad Politécnica de Madrid (2010) [<http://oa.upm.es/3669/>].
- ¹⁸M. van Schilfhaarde, T. Kotani, and S. Faleev, *Phys. Rev. Lett.* **96**, 226402 (2006).
- ¹⁹T. M. Henderson, A. F. Izmaylov, G. Scalmani, and G. E. Scuseria, *J. Chem. Phys.* **131**, 044108 (2009).
- ²⁰A. V. Krukau, O. A. Vydrov, A. F. Izmaylov, and G. E. Scuseria, *J. Chem. Phys.* **125**, 224106 (2006).
- ²¹J. Heyd, G. E. Scuseria, and M. Ernzerhof, *J. Chem. Phys.* **118**, 8207 (2003).
- ²²A. Stroppa, G. Kresse, and A. Continenza, *Phys. Rev. B* **83**, 085201 (2011).
- ²³A. F. Izmaylov, E. N. Brothers, and G. E. Scuseria, *J. Chem. Phys.* **125**, 224105 (2006); J. Heyd, J. E. Peralta, G. E. Scuseria, and R. L. Martin, *ibid.* **123**, 174101 (2005); J. Heyd and G. E. Scuseria, *ibid.* **120**, 7274 (2004); **121**, 1187 (2004).
- ²⁴J. Pohl and K. Albe, *J. Appl. Phys.* **108**, 023509 (2010).

- ²⁵B. G. Janesko, T. M. Henderson, and G. E. Scuseria, *Phys. Chem. Chem. Phys.* **11**, 443 (2009); T. M. Henderson, J. Paier, and G. E. Scuseria, *Phys. Status Solidi B* **248**, 767 (2011).
- ²⁶E. N. Brothers, A. F. Izmaylov, J. O. Normand, V. Barone, and G. E. Scuseria, *J. Chem. Phys.* **129**, 011102 (2008).
- ²⁷2008 Featured Articles: (a) July 31, Solar Cell Material Can Soak Up More Sun, [<http://www.newscientist.com>]; (b) August 9, A Step Closer to a Next Generation of Solar Cells, [<http://technology4life.wordpress.com>]; (c) September 30, Technical Insights Report, Intermediate-Band Materials for Solar Cells, Profile of the work done on indium sulfide-based materials, [www.frost.com].
- ²⁸T. F. W. Barth and E. Posnjak, *Z. Krist.* **82**, 325 (1932).
- ²⁹K. E. Sickafus and J. M. Wills, *J. Am. Ceram. Soc.* **82**, 3279 (1999).
- ³⁰E. J. W. Verwey and E. L. Heilman, *J. Chem. Phys.* **15**, 174 (1947).
- ³¹K. N. Kudin and G. E. Scuseria, *Phys. Rev. B* **61**, 16440 (2000).
- ³²K. N. Kudin and G. E. Scuseria, *Chem. Phys. Lett.* **289**, 611 (1998).
- ³³K. N. Kudin and G. E. Scuseria, *Chem. Phys. Lett.* **283**, 61 (1998).
- ³⁴M. J. Frisch, G. W. Trucks, H. B. Schlegel, G. E. Scuseria, M. A. Robb, J. R. Cheeseman, G. Scalmani, V. Barone, B. Mennucci, G. A. Petersson, H. Nakatsuji, M. Caricato, X. Li, H. P. Hratchian, A. F. Izmaylov, J. Bloino, G. Zheng, J. L. Sonnenberg, M. Hada, M. Ehara, K. Toyota, R. Fukuda, J. Hasegawa, M. Ishida, T. Nakajima, Y. Honda, O. Kitao, H. Nakai, T. Vreven, J. A. Montgomery Jr., J. E. Peralta, F. Ogliaro, M. Bearpark, J. J. Heyd, E. Brothers, K. N. Kudin, V. N. Staroverov, R. Kobayashi, J. Normand, K. Raghavachari, A. Rendell, J. C. Burant, S. S. Iyengar, J. Tomasi, M. Cossi, N. Rega, J. M. Millam, M. Klene, J. E. Knox, J. B. Cross, V. Bakken, C. Adamo, J. Jaramillo, R. Gomperts, R. E. Stratmann, O. Yazyev, A. J. Austin, R. Cammi, C. Pomelli, J. W. Ochterski, R. L. Martin, K. Morokuma, V. G. Zakrzewski, G. A. Voth, P. Salvador, J. J. Dannenberg, S. Dapprich, A. D. Daniels, O. Farkas, J. B. Foresman, J. V. Ortiz, J. Cioslowski, and D. J. Fox, *Gaussian 09 Revision A.1* (Gaussian Inc., Wallingford, CT, 2009).
- ³⁵R. Dennington II, T. Keith, and J. Millam, *GaussView 5.0* (Semichem, Inc., Wallingford, CT, 2000).
- ³⁶W. Humphrey, A. Dalke, and K. Schulten, *J. Mol. Graph.* **14**, 33 (1996), VMD—Visual Molecular Dynamics, version 1.8.7.
- ³⁷See supplemental material at [<http://link.aps.org/supplemental/10.1103/PhysRevB.83.205128>] for modified basis sets, information about pseudopotential generation, and high resolution graphics of the 56-atom unit cells.
- ³⁸ICSD, Inorganic Crystallographic Structural Database [www.fiz-karlsruhe.de/icsd_web.html] (2010).
- ³⁹K. N. Kudin, G. E. Scuseria, and H. B. Schlegel, *J. Chem. Phys.* **114**, 2919 (2001).
- ⁴⁰J. P. Perdew and Y. Wang, *Phys. Rev. B* **45**, 13244 (1992).
- ⁴¹S. H. Vosko, L. Wilk, and M. Nusair, *Can. J. Phys.* **58**, 1200 (1980).
- ⁴²J. P. Perdew, K. Burke, and M. Ernzerhof, *Phys. Rev. Lett.* **77**, 3865 (1996).
- ⁴³J. P. Perdew, K. Burke, and M. Ernzerhof, *Phys. Rev. Lett.* **78**, 1396 (1997).
- ⁴⁴J. Tao, J. P. Perdew, V. N. Staroverov, and G. E. Scuseria, *Phys. Rev. Lett.* **91**, 146401 (2003).
- ⁴⁵Specifically, we use the HSEh parametrization (Ref. 19) of HSE06 (Ref. 20) and (Ref. 21), called by the GAUSSIAN keyword HSEh1PBE.
- ⁴⁶X. Gonze, B. Amadon, P.-M. Anglade, J.-M. Beuken, F. Bottin, P. Boulanger, F. Bruneval, D. Caliste, R. Caracas, M. Cote, T. Deutsch, L. Genovese, P. Ghosez, M. Giantomassi, S. Goedecker, D. R. Hamann, P. Hermet, F. Jollet, G. Jomard, S. Leroux, M. Mancini, S. Mazevet, M. J. T. Oliveira, G. Onida, Y. Pouillon, T. Rangel, G.-M. Rignanese, D. Sangalli, R. Shaltaf, M. Torrent, M. J. Verstraete, G. Zerah, and J. W. Zwanziger, *Comput. Phys. Commun.* **180**, 2582 (2009), ABINIT.
- ⁴⁷M. Torrent, F. Jollet, F. Bottin, G. Zerah, and X. Gonze, *Comput. Mater. Sci.* **42**, 337 (2008).
- ⁴⁸G. B. Bachelet, D. R. Hamann, and M. Schluter, *Phys. Rev. B* **26**, 4199 (1982).
- ⁴⁹M. Fuchs and M. Scheffler, *Comput. Phys. Commun.* **119**, 67 (1999).
- ⁵⁰M. S. Hybertsen and S. G. Louie, *Phys. Rev. B* **34**, 5390 (1986).
- ⁵¹R. W. Godby and R. J. Needs, *Phys. Rev. Lett.* **62**, 1169 (1989).
- ⁵²S. N. Baek, T. S. Jeong, C. J. Youn, K. J. Hong, J. S. Park, D. C. Shin, and Y. T. Yoo, *J. Cryst. Growth* **262**, 259 (2004).
- ⁵³H. Nakanishi, *Jpn. J. Appl. Phys.* **19**, 103 (1980).
- ⁵⁴S. I. Radautsan, V. F. Zhitar, I. G. Kosnichan, M. I. Shmiglyuk, *Fiz. Tekh. Poluprovodn.* **5** (1971) 2240; *Sov. Phys. Semicond. (English Transl.)* **5** (1971) 1959.
- ⁵⁵W. Czaja and L. Krautsbauer, *Phys. Status Solidi* **33**, 191 (1969).
- ⁵⁶M. R. Brown, M. D. Martin, and W. A. Shand, *J. Phys. C* **3**, 1329 (1970).
- ⁵⁷Y. Li, R. Dillert, and D. Bahnemann, *Thin Solid Films* **516**, 4988 (2008).
- ⁵⁸J. Ruiz-Fuertes, D. Errandonea, F. J. Manjon, D. Martinez-Garcia, A. Segura, V. V. Ursaki, and I. M. Tiginyanu, *J. Appl. Phys.* **103**, 063710 (2008).
- ⁵⁹L. Betancourt, V. Sagredo, C. Rincon, and G. E. Delgado, *Rev. Mex. Fis.* **52**, 164 (2006).
- ⁶⁰S.-J. Lee, J.-E. Kim, and H.-Y. Park, *J. Mater. Res.* **18**, 733 (2003).
- ⁶¹M. Marinelli, S. Baroni, and F. Meloni, *Phys. Rev. B* **38**, 8258 (1988).
- ⁶²M. Bohm, G. Huber, A. MacKinnon, and O. Madelung, *Semiconductors Subvolume H: Physics of Ternary Compounds*, Landolt-Bornstein Numerical Data and Functional Relationships in Science and Technology, New Series, Group III, Vol. 17 (Springer-Verlag, New York, 1985), and references therein. See p. 137.
- ⁶³G. van Veen and R. D. Beer, *J. Phys. Chem. Solids* **38**, 217 (1977).
- ⁶⁴H. Nakanishi, S. Endo, and T. Irie, *J. Phys. (Paris) Colloq.* **36**, C3 (1975); see also *Jpn. J. Appl. Phys.* **19**, 103 (1980).
- ⁶⁵J. A. Beun, R. Nitsche, and M. Lichtensteiger, *Physica* **26**, 647 (1960).
- ⁶⁶H. Koelmans and H. G. Grimmeiss, *Physica* **25**, 1287 (1959).
- ⁶⁷T. Pisarkiewicz, K. Zakrzewska, and E. Leja, *Thin Solid Films* **153**, 479 (1987).
- ⁶⁸A. J. Nozik, *Phys. Rev. B* **6**, 453 (1972).
- ⁶⁹D. R. Kammler, T. O. Mason, D. L. Young, T. J. Coutts, D. Ko, K. R. Poepelmeier, and D. L. Williamson, *J. Appl. Phys.* **90**, 5979 (2001).
- ⁷⁰E. Burstein, *Phys. Rev.* **93**, 632 (1954); T. S. Moss, *Proc. Phys. Soc. London, B* **67**, 775 (1954).
- ⁷¹L. N. Brewer, D. R. Kammler, T. O. Mason, and V. P. Dravid, *J. Appl. Phys.* **89**, 951 (2001).
- ⁷²H. Hahn and W. Klinger, *Z. Anorg. Allg. Chem.* **263**, 177 (1950).
- ⁷³I. Aguilera, P. Palacios, K. Sánchez, and P. Wahnón, *Phys. Rev. B* **81**, 075206 (2010).

- ⁷⁴N. Barreau, A. Mokrani, F. Couzinié-Devy, and J. Kessler, *Thin Solid Films* **517**, 2316 (2009).
- ⁷⁵N. Barreau, *Solar Energy* **83**, 363 (2009).
- ⁷⁶F. Cerrina, C. Quaresima, I. Abbati, L. Braicovich, P. Picco, and G. Margaritondo, *Solid State Commun.* **33**, 429 (1980).
- ⁷⁷S. K. Apte, S. N. Garaje, R. D. Bolade, J. D. Ambekar, M. V. Kulkarni, S. D. Naik, S. W. Gosavi, J. O. Baeg, and B. B. Kale, *J. Mater. Chem.* **20**, 6095 (2010).
- ⁷⁸L. Schmicka, J. Harl, and G. Kresse, *J. Chem. Phys.* **134**, 024116 (2011).
- ⁷⁹E. R. Batista, J. Heyd, R. G. Hennig, B. P. Uberuaga, R. L. Martin, G. E. Scuseria, C. J. Umrigar, and J. W. Wilkins, *Phys. Rev. B* **74**, 121102 (2006).
- ⁸⁰D. O. Scanlon, B. J. Morgan, G. W. Watson, and A. Walsh, *Phys. Rev. Lett.* **103**, 096405 (2009).
- ⁸¹S.-H. Wei and S. B. Zhang, *Phys. Rev. B* **63**, 045112 (2001).
- ⁸²M. Womes, J. C. Jumas, and J. Olivier-Fourcade, *Solid State Commun.* **131**, 257 (2004).
- ⁸³N. Barreau, J. C. Bernède, S. Marsillac, and A. Mokrani, *J. Cryst. Growth* **235**, 439 (2002).
- ⁸⁴G. D. Price, S. L. Price, and J. K. Burdett, *Phys. Chem. Miner.* **8**, 69 (1982).
- ⁸⁵U. Schmocker, H. R. Boesch, and F. Waldner, *Phys. Lett.* **40A**, 237 (1972).
- ⁸⁶R. J. Hill, J. R. Craig, and G. V. Gibbs, *Phys. Chem. Miner.* **4**, 317 (1979).
- ⁸⁷G. D. Price and N. L. Ross, *The Stability of Minerals*, Mineralogical Society Series Vol. 3 (Chapman & Hall, New York, 1992).
- ⁸⁸M. O'Keefe and B. G. Hyde, *Cation Ordering and Electron Transfer Structure and Bonding* **61**, 77 (1985).
- ⁸⁹J. C. Deelman, *Neues Jb. Miner. Monat.* **7**, 289 (1999).
- ⁹⁰T. Threlfall, *Org. Proc. Res. Dev.* **7**, 1017 (2003).
- ⁹¹A. Seko, K. Yuge, F. Oba, A. Kuwabara, and I. Tanaka, *Phys. Rev. B* **73**, 184117 (2006).
- ⁹²A. Putnis, *Introduction to Mineral Sciences* (Cambridge University Press, NY, NY 40 w. 20th Street 1992).
- ⁹³A. Seko, F. Oba, and I. Tanaka, *Phys. Rev. B* **81**, 054114 (2010).
- ⁹⁴H. Schmalzried, *Z. Phys. Chem.* **28**, 203 (1961); J. E. Wiedenborner, N. Stemple, and Y. Okaya, *Acta Crystallogr.* **20**, 761 (1966).
- ⁹⁵V. Stevanović, M. d'Avezac, and A. Zunger, *Phys. Rev. Lett.* **105**, 075501 (2010).
- ⁹⁶A. Seko, K. Yuge, F. Oba, A. Kuwabara, I. Tanaka, and T. Yamamoto, *Phys. Rev. B* **73**, 094116 (2006), and references therein.
- ⁹⁷A. Zunger, in *Statistics and Dynamics of Alloy Phase Transformations*, Rhodes, 1993, edited by P. E. A. Turchi and A. Gonis (Plenum, New York, 1994).
- ⁹⁸F. Semari, R. Khenata, M. Rabah, A. Bouhemadou, S. B. Omran, A. H. Reshak, and D. Rached, *J. Solid State Chem.* **183**, 2818 (2010).
- ⁹⁹P. Palacios, I. Aguilera, K. Sánchez, J. C. Conesa, and P. Wahnón, *Phys. Rev. Lett.* **101**, 046403 (2008).
- ¹⁰⁰B. Li, L. Zeng, and F. Zhang, *Phys. Status Solidi A* **201**, 960 (2004).
- ¹⁰¹V. V. Ursaki, F. Manjón, I. Tiginyanu, and V. E. Tezlevan, *J. Phys. Condens. Matter* **14**, 6801 (2002).
- ¹⁰²S. Katsuki, *Solid State Commun.* **39**, 767 (1981).
- ¹⁰³M. Wakaki, O. Shintani, T. Ogawa, and T. Arai, *Jpn. J. Appl. Phys.* **19S3**, 255 (1980).
- ¹⁰⁴D. Fiorani and S. Viticoli, *Solid State Commun.* **32**, 889 (1979).
- ¹⁰⁵L. Gastaldi and A. Lapicciarella, *J. Solid State Chem.* **30**, 223 (1979).
- ¹⁰⁶P. M. Sirimanne, N. Sonoyama, and T. Sakata, *J. Solid State Chem.* **154**, 476 (2000).
- ¹⁰⁷E. Fortin, S. Fafard, A. Anedda, F. Ledda, and A. Charlebois, *Solid State Commun.* **77**, 165 (1991).
- ¹⁰⁸R. Dedryvere, P. E. Lippens, J. C. Jumas, I. Lefebvre-Devos, and C. P. Vicente, *Solid State Sci.* **3**, 267 (2001).
- ¹⁰⁹D. J. Singh, R. C. Rai, J. L. Musfeldt, S. Auluck, N. Singh, P. Khalifah, S. McClure, D. G. Mandrus, W. Shockley, and H. J. Queisser, *Chem. Mater.* **18**, 2696 (2006).
- ¹¹⁰L. Pisani, T. Maitra, and R. Valenti, *Phys. Rev. B* **73**, 205204 (2006).
- ¹¹¹F. Urbach, *Phys. Rev.* **92**, 1324 (1953).
- ¹¹²D. A. Drabold, Y. Li, B. Cai, and M. Zhang, *Phys. Rev. B* **83**, 045201 (2011), and references therein.
- ¹¹³W. Setywan and S. Curtarolo, *Comput. Mater. Sci.* **49**, 299 (2010).
- ¹¹⁴N. Mansourian-Hadavi, S. Wansom, N. H. Perry, A. R. Nagaraja, T. O. Mason, L. H. Ye, and A. J. Freeman, *Phys. Rev. B* **81**, 075112 (2010).
- ¹¹⁵S. Lopez, A. H. Romero, P. Rodriguez-Hernandez, and A. Munoz, *Phys. Rev. B* **79**, 214103 (2009).
- ¹¹⁶F. Trani, J. Vidal, S. Botti, and M. A. L. Marques, *Phys. Rev. B* **82**, 085115 (2010); **83**, 039901(E) (2011).
- ¹¹⁷S. Botti, F. Sottile, N. Vast, V. Olevano, L. Reining, H. C. Weissker, A. Rubio, G. Onida, R. DelSole, and R. W. Godby, *Phys. Rev. B* **69**, 155112 (2004).
- ¹¹⁸G. D. Mahan, *Many Particle Physics (Physics of Solids and Liquids)* 3rd ed. (Springer, 2000).
- ¹¹⁹M. Wakaki, O. Shintani, T. Ogawa, and T. Arai, *Jpn. J. Appl. Phys.* **21**, 958 (1982).
- ¹²⁰N. Syrбу, M. Bogdanash, and N. A. Moldovyan, *Infrared Phys. Technol.* **37**, 763 (1996).
- ¹²¹J. Vidal, F. Trani, F. Bruneval, M. A. L. Marques, and S. Botti, *Phys. Rev. Lett.* **104**, 136401 (2010).
- ¹²²A. Stroppa, M. Marsman, G. Kresse, and S. Picozzi, *New J. Phys.* **12**, 13 (2010).
- ¹²³Y.-S. Kim, K. Hummer, and G. Kresse, *Phys. Rev. B* **80**, 035203 (2009).